Two-Phase Flow in the Vicinity of an Elongated Bubble in a Fluidized Bed

Yeshayahou Levy and Yuri Dorfman
Faculty of Aerospace Engineering, Technion—Israel Institute of Technology, Haifa 32000, Israel

Fluid and solid dynamics inside and outside a stable elongated gas bubble in operating conditions corresponding to those of the channeling regime in a fluidized bed are described. It considers the prolate ellipsoid of revolution as a model of the bubble. The results of the analytical model show a significant increase of the fluid velocity inside the bubble with the growth of its relative height. The maximum values of the fluid velocities exist along the vertical axis of the bubble. For the limiting case of a spherical bubble, the fluid and gas performance, such as the existence of a surface of penetration outside the bubble boundaries and circulation zone inside the bubble, are in good agreement with the existing theory.

Introduction

Experience in fluidization shows that an increase of fluid flow through the fluidized bed beyond the bubbling regime causes channeling where the shape of the bubble significantly differs from the sphere and becomes elongated.

The objective of the present paper is to obtain a theoretical description of the fluid and solid flows both outside and inside the elongated bubble. The description is based on the approximation of the elongated bubble surface with that of the prolate ellipsoid of revolution. The interaction between fluid, solids, and bubble boundary is considered using fluid mechanics theory and the model introduced by Davidson (1961).

The present paper shows an essential increase of the vertical fluid velocity inside the elongated bubble with growth of its relative height. It was found that the maximum velocity values occur in the center of the elongated bubble.

The solution for the fluid velocity distribution inside the elongated bubble may be useful for a pressure analysis, required for describing the bubble's behavior in unsteady conditions of its rising and its further bursting at the fluidized bed surface. As a result of the velocity increase inside the bubble, an increase in the velocity of the solids ejected into the freeboard can be predicted. This may cause a dominant contribution to the turbulent intensity growth in the freeboard that must be taken into consideration when analyzing the elutriation process in fluidized beds.

Correspondence concerning this article should be addressed to Dr. Y. Levy, Faculty of Aerospace Engineering, Technion—Israel Institute of Technology, Haifa 32000, Israel.

The model presented concerns the two-phase flow characteristics in the vicinity of a prolate ellipsoid of revolution. It can be used to describe the behavior of a steady-state gas bubble under conditions corresponding to those of the channeling regime in the fluidized bed. The model allows us to obtain a mathematical description of the fluid and solid flows inside and outside the bubble.

When we extend the elliptical shape of the bubble to that of a sphere, our results are in exact agreement with those of Davidson and Harrison (1963) and Pyle and Rose (1965). For a prolate ellipsoid of revolution the general behavior is of similar characteristics to that of a spherical bubble. This concerns the velocity and pressure values in some principal points, such as the central and top points, in the penetration zone outside the bubble, and in the circulation zone inside the bubble.

A simple equation for the cross-sectional mean vertical velocity inside the bubble was obtained. The main difference in the two-phase flow between that of elliptical and spherical bubbles is in the relative values of the internal fluid velocity. There is a significant and nonlinear increase of the mean vertical velocity with the relative height of the bubble. This leads to the rapid growth of the fluid velocity inside an elongated bubble in comparison with that of a spherical shape. The velocity can obtain a typical value of tens of m/s in typical conditions of fluidization. The maximum velocity value in the bubble is in its center and increases with the relative bubble height. Hence, the main conclusion is that in the channeling

regime of a fluidization, the ejection velocities of particles into the freeboard (affected by the internal velocity in the bubble) can be much greater than in the bubbling regime of fluidization. This may at least partially explain the differences between the predicted and measured amount of solids elutriated from fluidized beds.

Previous work

The physical principles of the two-phase flow behavior in the vicinity of a spherical bubble were summarized by Davidson and Harrison (1963). We shall repeat and organize them for convenience, using rectangular coordinates.

The solid phase is considered to be an incompressible fluid with the bulk density equal to that of the bed at incipient fluidization. This follows from the assumption that all the excess fluid above minimum fluidization passes through as bubbles. The continuity equation for the solid particles is

$$\frac{\partial V_x}{\partial x}+\frac{\partial V_y}{\partial y}=0, \tag{1}$$

where x, y are the rectangular coordinates, with the origin placed in the bubble center, and V_x, V_y are the solids' velocity components.

The components of the absolute fluid velocity U_x, U_y are represented as a sum of the solids' velocities V_x, V_y and the relative velocities between the fluidizing fluid and solids W_x, W_y

$$U_x=V_x+W_x$$
$$U_y=V_y+W_y. \tag{2}$$

The continuity equation for the fluidizing fluid, which is considered incompressible, is

$$\frac{\partial U_x}{\partial x}+\frac{\partial U_y}{\partial y}=0. \tag{3}$$

From Eqs. 1-3

$$\frac{\partial W_x}{\partial x}+\frac{\partial W_y}{\partial y}=0. \tag{4}$$

The relative velocity between the fluidizing fluid and solids is assumed to be proportional to the pressure P_f gradient within the fluidizing fluid in accordance with Darcy's law for percolation of fluid through fixed beds of particles or barrier filters:

$$W_x=-\kappa\frac{\partial P_f}{\partial x}$$
$$W_y=-\kappa\frac{\partial P_f}{\partial y}, \tag{5}$$

where κ is a constant, being a characteristic of the particles and of the fluidizing fluid.

From Eqs. 4 and 5 we obtain an equation for pressure distribution within the fluidizing fluid that is independent of the solids' motion

$$\frac{\partial^2(\kappa P_f)}{\partial x^2}+\frac{\partial^2(\kappa P_f)}{\partial y^2}=0, \tag{6}$$

and has the following boundary conditions:

P_f = constant at the surface of the bubble;
grad P_f = constant at infinity.

The motion of the solid phase is considered to be a potential motion with velocity V relative to the gas bubble. The solution for the velocity potential ϕ_V is based on the assumption that the bubbles can be described by solid bodies (since the solids do not penetrate into the bubble). ϕ_V is known from the theory of potential flows for a few different body shapes. So for the relative particle velocity we obtain

$$V_x=\frac{\partial\phi_V}{\partial x}$$
$$V_y=\frac{\partial\phi_V}{\partial y}. \tag{7}$$

The relative motion between the fluidizing fluid and solids (W) is described by Eqs. 5 and 6. According to Eq. 5, the gradient of the function $-\kappa P_f$ is equal to the velocity W. Equation 6 represents Laplace's equation for the function $-\kappa P_f$. Hence, the function $-\kappa P_f$ corresponds to the properties of velocity potential, and so the relative motion between the fluidizing fluid and solids also has potential denoted as ϕ_W with boundary conditions such as those of Eq. 6:

ϕ_W = constant at the surface of the bubble;
grad ϕ_W = constant at infinity.

The solution for this potential can be obtained for few bubble shapes.

The flow of the fluidizing fluid described in a coordinate system with its origin placed in the center of the bubble cannot *a priori* be considered as a potential flow; so its velocity can be connected only with stream function Ψ_u:

$$U_x=\frac{\partial\Psi_u}{\partial y}$$
$$U_y=\frac{\partial\Psi_u}{\partial x}. \tag{8}$$

The solution of Ψ_u can be obtained through Eq. 2 by using the just mentioned equations for ϕ_V and $-\kappa P_f$.

Davidson and Harrison (1963) obtained this solution for two and three dimensions, namely, for a cylinder with a circular cross section and for a sphere. Grace and Harrison (1969) presented a solution in elliptic coordinates for a cylinder with an elliptic cross section.

Theory

Flow of solids and fluid around an elongated bubble

In operating conditions that correspond to those of the channeling regime of fluidization the gas bubble acquires the shape of an elongated body. In a three-dimensional fluidized bed this body may have an axis of symmetry in the vertical direction. A good mathematical representation of such a shape is the prolate ellipsoid of revolution.

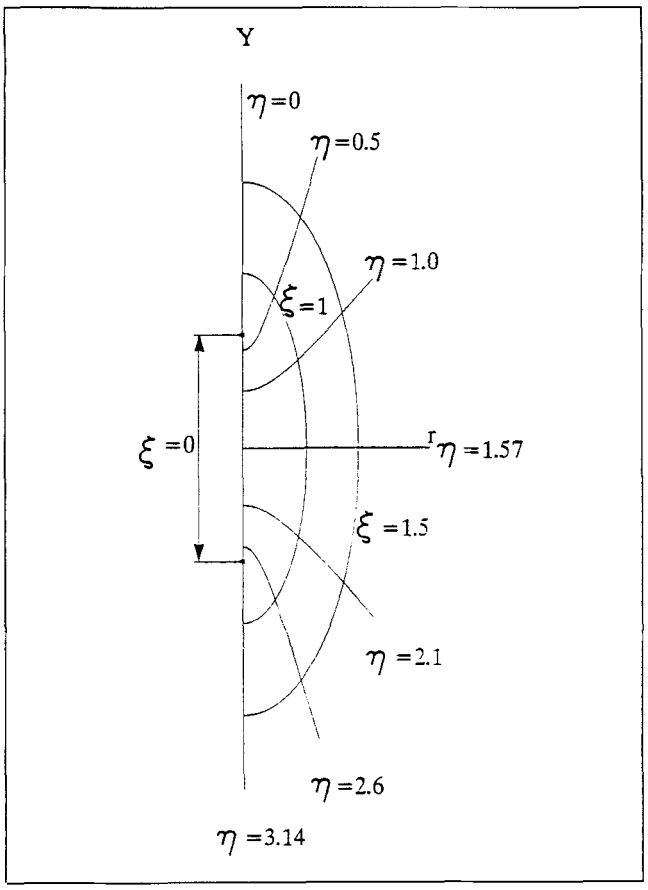

Figure 1. Elliptic coordinates.

Consider an elliptic coordinate system ξ, η with the ranges (see Figure 1)

$$0 \le \xi \le \infty$$

$$0 \le \eta \le \pi.$$

Using the relation

$$\cos(\xi + i\eta) = \frac{1}{c}(y + ir)$$

we obtain

$$y = c \cosh \xi \cos \eta$$

$$r = c \sinh \phi \sin \eta,$$

where y is the vertical coordinate (see Figure 2), r is the radius of the ellipsoid cross section, and c is the eccentricity of the ellipsoid.

In addition, we define a new coordinate system:

$$\lambda = \cosh \xi \qquad 1 \le \lambda < \infty$$

$$\mu = \cos \eta \qquad -1 \le \mu \le 1$$

and $\lambda = \lambda_0$ at the ellipsoid representing the bubble surface. Hence.

$$y = c\lambda\mu$$

$$r = c(\lambda^2 - 1)^{1/2}(1 - \mu^2)^{1/2}. \tag{9}$$

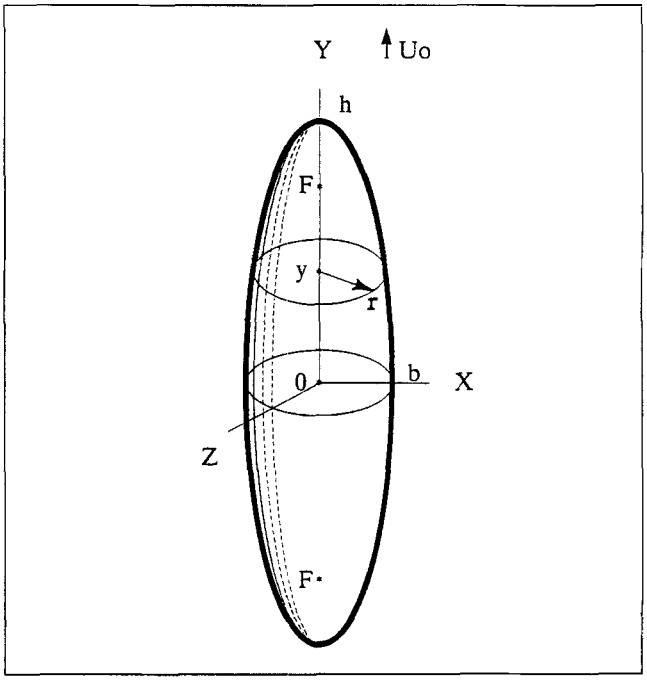

Figure 2. Ellipsoid bubble.

Using the coordinate system λ, μ instead of ξ, η, the Laplace's equation for the velocity potential is (Lamb, 1945)

$$\frac{\partial}{\partial\lambda}\left[(\lambda^2 - 1)\frac{\partial\phi}{\partial\lambda}\right] + \frac{\partial}{\partial\mu}\left[(1 - \mu^2)\frac{\partial\phi}{\partial\mu}\right] = 0. \tag{10}$$

Relative Velocity between Solids and Fluidizing Fluid. We shall solve Laplace's Eq. 10 for the relative motion between the fluidizing fluid and solids, where the velocity potential ϕ_W is represented as

$$\phi_W = -\kappa P_f. \tag{11}$$

The boundary conditions are in accordance with the pressure distribution in the fluidized bed:

$$-\kappa P_f(\lambda_0) = \text{cons.}$$

$$\text{grad} - \kappa P_f(\lambda \to \infty) = U_0, \tag{12}$$

where U_0 is the gas velocity at minimum fluidization, which represents the relative velocity between solids and gas at infinity.

The solution of Laplace's Eq. 10 is (Lamb, 1945)

$$-\kappa P_f = cU_0\left[\sum_{n=1}^{\infty} A_n Q_n(\lambda) P_n(\mu) + \lambda\mu\right], \tag{13}$$

where A_n are constant coefficients that depend on the boundary conditions, and $P_n(x)$, $Q_n(x)$ are Legendre's functions of the first and second kind.

Using the assumption that $A_n = 0$ for $n > 1$, and the first boundary condition from 12

$$-\kappa P_f(\lambda_0) = cU_0[A_1 Q_1(\lambda_0) P_1(\mu) + \lambda_0 \mu] = 0, \qquad (14)$$

(as zero also represents a constant), and knowing that

$$P_1(x) = x$$

$$Q_1(x) = \frac{1}{2} x \ln \frac{x+1}{x-1} - 1,$$

we shall receive

$$A_1 = -\frac{\lambda_0}{\frac{\lambda_0}{2} \ln \frac{\lambda_0+1}{\lambda_0-1} - 1}.$$

Then, from Eq. 13 we obtain the formula for pressure distribution around the bubble:

$$P_f = \frac{cU_0}{\kappa} \lambda\mu \left(\frac{\frac{\lambda_0}{2} \ln \frac{\lambda+1}{\lambda-1} - \frac{\lambda_0}{\lambda}}{\frac{\lambda_0}{2} \ln \frac{\lambda_0+1}{\lambda_0-1} - 1} - 1 \right). \qquad (15)$$

This equation also represents a solution of Laplace's equation (Eq. 10) for the relative velocity W, satisfying the boundary conditions 12. According to the first boundary condition, Eq. 15 may represent the pressure difference relative to the bubble boundary, although in practice pressure at the boundary is constant and positive. Equation 15 can also be used in the specific case of a spherical bubble, which is obtained when λ, $\lambda_0 \to \infty$ (or $c \to 0$). In this case we shall receive

$$P_f = -\frac{cU_0}{\kappa} \lambda\mu \left(1 - \frac{\lambda_0^3}{\lambda^3}\right) = -\frac{U_0}{\kappa} \left(r - \frac{b^3}{r^2}\right) \cos \eta,$$

where b is the radius of a spherical bubble, and r is the radial coordinate. Using the general relation between stream function Ψ and velocity potential ϕ for elliptic coordinates (Lamb, 1945)

$$\frac{\partial \Psi}{\partial \mu} = c(\lambda^2 - 1) \frac{\partial \phi}{\partial \lambda}, \qquad (16)$$

we can obtain

$$\Psi_w = -c^2(\lambda^2 - 1) \frac{1-\mu^2}{2} U_0 \left(\frac{\frac{\lambda_0}{2} \ln \frac{\lambda+1}{\lambda-1} - \frac{\lambda_0 \lambda}{\lambda^2-1}}{\frac{\lambda_0}{2} \ln \frac{\lambda_0+1}{\lambda_0-1} - 1} - 1 \right). \qquad (17)$$

This equation also satisfies the solution for a spherical bubble (Davidson and Harrison, 1963), where λ, $\lambda_0 \to \infty$

$$\Psi_w = -c^2\lambda^2 \frac{(1-\mu^2)}{2} U_0 \left(1 + 2\frac{\lambda_0^3}{\lambda^3}\right) = -U_0 \left(1 + \frac{2b^3}{r^3}\right) \frac{r^2}{2} \sin^2 \eta.$$

The stream function obtained by solution 17 can be used to determine the fluid flow penetrating the ellipsoidal bubble. On its surface, when $\lambda = \lambda_0$ we obtain

$$\Psi_w = c^2 \left(\frac{1-\mu^2}{2}\right) \frac{U_0}{\frac{\lambda_0}{2} \ln \frac{\lambda_0+1}{\lambda_0-1} - 1}. \qquad (18)$$

Since $2\pi\epsilon\Psi_w = q$ is the fluid flow rate,

$$q = \frac{\pi U_0 c^2 (1-\mu^2)\epsilon}{\frac{\lambda_0}{2} \ln \frac{\lambda_0+1}{\lambda_0-1} - 1}, \qquad (19)$$

where ϵ is the voidage coefficient.

We can evaluate the mean flow velocity U_c inside the ellipsoidal bubble by using Eq. 19 and the local cross section area πr^2 with r from Eq. 9:

$$U_c = U_{mf} \frac{\frac{1}{\lambda_0^2 - 1}}{\frac{\lambda_0}{2} \ln \frac{\lambda_0+1}{\lambda_0-1} - 1}, \qquad (20)$$

where $U_{mf} = U_0 \epsilon$ is the minimum fluidizing velocity.

From this equation it is evident that the mean vertical velocity inside the bubble is constant at all cross sections. Hence we obtain a correlation between the mean vertical velocity inside the bubble and its geometrical property h/b

$$\frac{U_c}{U_{mf}} = \frac{(h/b)^2 - 1}{\frac{h/b}{2\sqrt{(h/b^2) - 1}} \ln \frac{h/b + \sqrt{(h/b)^2 - 1}}{h/b - \sqrt{(h/b)^2 - 1}} - 1},$$

where b, h are the width and height of the bubble, respectively.

Solid phase velocity. Laplace's equation (Eq. 10) for the solid phase can be solved using the boundary condition $\Psi_v(\lambda_0) = 0$, that is, that the stream functions on the bubble boundary are equal to zero, or equivalently, that the solid phase does not penetrate the bubble. The solution is (Lamb, 1945)

$$\phi_V = -cU_b\mu \left(\frac{\frac{\lambda}{2} \ln \frac{\lambda+1}{\lambda-1} - 1}{\frac{1}{2} \ln \frac{\lambda_0+1}{\lambda_0-1} - \frac{\lambda_0}{\lambda_0^2-1}} - \lambda \right),$$

where U_b is the bubble rise velocity.

Fluid velocity. The absolute fluid velocity normal to ellipsoid surface

$$U_\lambda(\mu,\lambda)_o = V_\lambda(\mu,\lambda)_o + W_\lambda(\mu,\lambda)_o, \qquad (21)$$

and the correlation between velocities $V_\lambda(\mu,\lambda)_o$, $W_\lambda(\mu,\lambda)_o$ and their potentials ϕ_V, $\phi_w = -\kappa P_f$ is (Lamb, 1945)

$$V_\lambda(\mu,\lambda)_o = \frac{1}{c} \sqrt{\frac{\lambda^2-1}{\lambda^2-\mu^2}} \frac{\partial \phi_V}{\partial \lambda}$$

$$W_\lambda(\mu,\lambda)_o=\frac{1}{c}\sqrt{\frac{\lambda^2-1}{\lambda^2-\mu^2}}\frac{\partial(-\kappa P_f)}{\partial\lambda},$$

where o denotes outside the bubble boundary.

For the absolute fluid velocity we shall use the relation between $U_\lambda(\mu,\lambda)_o$ and stream function Ψ_u (Lamb, 1945)

$$U_\lambda(\mu,\lambda)_o=\frac{1}{c^2\sqrt{(\lambda^2-\mu^2)(\lambda^2-1)}}\frac{\partial\Psi_u}{\partial\mu}. \tag{22}$$

Combining the three last equations in 21 we obtain an equation for fluid flow stream function

$$\frac{\partial\Psi_u}{\partial\mu}=c(\lambda^2-1)\left[\frac{\partial\phi_V}{\partial\lambda}-\frac{\partial\kappa P_f}{\partial\lambda}\right],$$

or after integration from 1 to μ,

$$\Psi_u=-c^2\frac{\lambda^2-1}{2}(1-\mu^2)U_0 \times\left\{(\overline{U}_b-1)-\frac{F(\lambda)}{F(\lambda_0)}[\overline{U}_b-G(\lambda_0)]\right\}. \tag{23}$$

We define

$$\overline{U}_b=\frac{U_b}{U_0}$$

$$F(x)=\frac{1}{2}\ln\frac{x+1}{x-1}-\frac{x}{x^2-1}$$

$$G(x)=\frac{1}{1+\dfrac{1}{F(x)(x^3-x)}}.$$

From solution 23 we can obtain conditions for the zero stream line, or an equation for the *surface of penetration*, the surface separating the flow that passes through the bubble and the fluidized bed flow

$$F(\lambda)=F(\lambda_0)\frac{\overline{U}_b-1}{\overline{U}_b-G(\lambda_0)}. \tag{24}$$

Fluid flow inside an elongated bubble

The main difference in the fluid motion between the inside of the bubble and its outside is that the inside flow is not a potential flow, due to the internal fluid circulation. Hence Laplace's equation may not be used for constructing the stream function.

Due to the fact that the bubble boundaries are transparent to fluid motion and the Reynolds numbers of the fluid flow relative to the solid particles that form the bubble boundaries are low (Re < 50), we may adopt the Stokes stream function, as was done by Pyle and Rose (1965) for the case of the spherical bubble. In the present study we assume similar behavior. Then the Stokes stream function is obtained from (Heppel and Brenner, 1965)

$$E^4\Psi=0, \tag{25}$$

where operator E^2 for elliptic coordinate systems, shown in Figure 1, can be written as

$$E^2=\frac{1}{c^2(\lambda^2-\mu^2)}\left[(\lambda^2-1)\frac{\partial^2}{\partial\lambda^2}+(1-\mu^2)\frac{\partial^2}{\partial\mu^2}\right].$$

The solution of Eq. 25 can be constructed in the form of

$$\Psi=Ac^2(\lambda^2-1)(B+c^2\lambda^2)(1-\mu^2), \tag{26}$$

where A and B are constant. The boundary conditions are

$$U_\lambda(\mu,\lambda_0)_i=\epsilon U_\lambda(\mu,\lambda_0)_o \qquad \text{(normal velocity)} \tag{27}$$

$$U_\mu(\mu,\lambda_0)_i=U_\mu(\mu,\lambda_0)_o \qquad \text{(tangential velocity)}, \tag{28}$$

where i denotes inside the bubble boundary (λ_0). As justification for condition 28, we can consider that the tangential fluid velocity outside the bubble on its boundary can be obtained using Eq. 23, since

$$U_\mu(\mu,\lambda_0)_o=\frac{1}{c^2\sqrt{(\lambda^2-\mu^2)(1-\mu^2)}}\frac{\partial\Psi_u}{\partial\lambda}\bigg|_{\lambda=\lambda_0} =U_b\lambda_0\sqrt{\frac{1-\mu^2}{\lambda_0^2-\mu^2}}\frac{1-G(\lambda_0)}{G(\lambda_0)}.$$

The same equation is derived for the solid velocity on the bubble boundary:

$$V_\mu(\mu,\lambda_0)_o=\frac{1}{c}\sqrt{\frac{1-\mu^2}{\lambda^2-\mu^2}}\frac{\partial\phi_V}{\partial\mu}\bigg|_{\lambda=\lambda_0} =U_b\lambda_0\sqrt{\frac{1-\mu^2}{\lambda_0^2-\mu^2}}\frac{1-G(\lambda_0)}{G(\lambda_0)}. \tag{29}$$

The result obtained is in accordance with the physical restriction that, as $P_f(\lambda_0)=0$ (see Eq. 15), the relative tangential velocity $W_\mu(\mu,\lambda_0)$ between fluid and solids is equal to zero.

Since the tangential velocities of the fluid and the solid on the outer surface of the bubble are equal, we can consider that the fluid tangential velocity inside the bubble is equal to that of the bubble surface (no slip conditions). Hence the relative velocity on the bubble surface just inside the bubble equals zero.

Using conditions 27 and 28 we can write two equations for the determination of the unknown coefficients A and B and obtain stream function inside the prolate ellipsoid of revolution as

$$\Psi_i=-c^2\epsilon U_0(1-\mu^2)\frac{\lambda^2-1}{2}\frac{G(\lambda_0)-1}{G(\lambda_0)} \times\left[\frac{G(\lambda_0)-\overline{U}_{b_\epsilon}}{\lambda_0^2-1}(\lambda_0^2-\lambda^2)+G(\lambda_0)\right], \tag{30}$$

where $\overline{U}_{b_\epsilon}=\overline{U}_b/\epsilon$.

Flow velocity inside the bubble. Using the relation between Cartesian and elliptic coordinates, the equation for the vertical velocity is

$$U_y(\mu,\lambda)_i=\frac{1}{\sqrt{\lambda^2-\mu^2}}\left(\mu U_\lambda(\mu,\lambda)_i\sqrt{\lambda^2-1}+\lambda U_\mu(\mu,\lambda)_i\sqrt{1-\mu^2}\right),$$

where

$$U_\lambda(\mu,\lambda)_i=\frac{1}{c^2\sqrt{(\lambda^2-\mu^2)(\lambda^2-1)}}\frac{\partial\Psi_i}{\partial\mu} \tag{31}$$

$$U_\mu(\mu,\lambda)_i=\frac{1}{c^2\sqrt{(\lambda^2-\mu^2)(1-\mu^2)}}\frac{\partial\Psi_i}{\partial\lambda}, \tag{32}$$

or by Eq. 30

$$U_y(\mu,\lambda)_i=\frac{\epsilon U_0}{\lambda^2-\mu^2}\frac{G(\lambda_0)-1}{G(\lambda_0)}\times\left\{\left[\frac{G(\lambda_0)-\overline{U}_{b_\epsilon}}{\lambda_0^2-1}(\lambda_0^2-\lambda^2)+G(\lambda_0)\right](\lambda^2-1)\mu^2+\left[\frac{G(\lambda_0)-\overline{U}_{b_\epsilon}}{\lambda_0^2-1}(\lambda_0^2-2\lambda^2+1)+G(\lambda_0)\right]\lambda^2(1-\mu^2)\right\}. \tag{33}$$

The vertical velocity in the central cross section [when $y=0$ (see Figure 2) and, hence $\mu=0$] is

$$U_y(0,\lambda)_i=\epsilon U_0\frac{G(\lambda_0)-1}{G(\lambda_0)}\times\left[\frac{G(\lambda_0)-\overline{U}_{b_\epsilon}}{\lambda_0^2-1}(\lambda_0^2-2\lambda^2+1)+G(\lambda_0)\right]. \tag{34}$$

This velocity can be equal to zero in the location where

$$\lambda^2-1=(\lambda_0^2-1)\frac{G(\lambda_0)-\frac{\overline{U}_{b_\epsilon}}{2}}{G(\lambda_0)-\overline{U}_{b_\epsilon}}.$$

We can see that as $G(\lambda_0)<0$ and $\overline{U}_{b_\epsilon}>0$, then $\lambda<\lambda_0$; hence, there always exists in the bubble an internal finite circulation zone of the fluid. The size of this circulation zone increases as $\overline{U}_{b_\epsilon}$ increases.

It is also of interest to determinate the vertical velocities on the y-axis in two principal points: the origin, where $\mu=0$ and $\lambda=1$

$$U_y(0,1)_i=U_{mf}[G(\lambda_0)-1]\left[2-\frac{\overline{U}_{b_\epsilon}}{G(\lambda_0)}\right],$$

and the top point of the bubble, where $\mu=1$ and $\lambda=\lambda_0$:

$$U_y(1,\lambda_0)_i=U_{mf}[G(\lambda_0)-1].$$

From an analysis of the function $G(\lambda_0)$ we can state that, as $G(\lambda_0)<0$ and $(2-[\overline{U}_{b_\epsilon}/G(\lambda_0)])>1$, the vertical velocity in the top point of the bubble will be less than that in the origin. This correlation also remains for a spherical bubble.

It can be shown that the value of $U_{yi}(1,\lambda_0)$ is identical to that from Eq. 20, derived when a circulation zone was not considered. The similarity of these equations follows from the fact that there is no circulation at the top point. It is of interest to consider the regime, when $\overline{U}_{b_\epsilon}=0$ ($U_b=0$), which corresponds to the absence of the circulation zone as also indicated by Pyle and Rose (1965). Then we can obtain the value for vertical velocity at the origin

$$U_y(0,1)_i=2U_c.$$

Hence, the mean vertical velocity U_c obtained previously in Eq. 20 can be used for a quick approximation of the actual velocity inside the bubble. Its value is equal to vertical velocity at the top point of the ellipsoidal bubble or to half of the vertical velocity in the origin in the absence of the circulation zone.

Pressure distribution inside the bubble. Using Eq. 15 for pressure distribution around the bubble we can write at infinity, where $\lambda\to\infty$,

$$P_f=-\frac{U_0}{\kappa}y.$$

Notice from this equation that at infinity the constant pressure curves become horizontal. We can therefore consider that this distribution corresponds to the stagnation pressure.

This curve for the constant pressure value can be easily calculated since it corresponds to the static pressure in the fluidized bed at a different depth that equals the distance between this curve at infinity and the bed surface. The dynamic pressure of the fluid at infinity is ignored due to its insignificance. We can define the stagnation pressure on the bubble boundary as

$$P_o=\rho_p(1-\epsilon)gH+P_{b.s}, \tag{35}$$

where H is the distance between the bubble center and the bed surface, and $P_{b.s}$ is the pressure above the bed surface. The stagnation pressure does not change all over the bubble boundary in accordance with Eq. 15. Assuming constant stagnation pressure in the bubble cavity, we may define the static pressure distribution inside the bubble as

$$P=\rho_p(1-\epsilon)gH+P_{b.s}-\rho_g\frac{U_i^2}{2}, \tag{36}$$

where ρ_g is the fluid density, and $U(\mu,\lambda)_i=(U_\lambda^2(\mu,\lambda)_i+U_\mu^2(\mu,\lambda)_i)^{1/2}$ is the absolute fluid velocity. Using Eqs. 31, 32, and 30, we can formulate the absolute velocity distribution inside an elliptic bubble:

$$\frac{U^2(\mu,\lambda)_i}{2}=\frac{\left[\epsilon U_o\,\frac{G(\lambda_0)-1}{G(\lambda_0)}\right]^2}{2(\lambda^2-\mu^2)}$$

$$\times\left\{\mu^2(\lambda^2-1)\left[\frac{G(\lambda_0)-\overline{U}_{b_\epsilon}}{\lambda_0^2-1}(\lambda_0^2-\lambda^2)+G(\lambda_0)\right]^2\right.$$

$$\left.+\lambda^2(1-\mu^2)\left[\frac{G(\lambda_0)-\overline{U}_{b_\epsilon}}{\lambda_0^2-1}(\lambda_0^2-2\lambda^2+1)+G(\lambda_0)\right]^2\right\}. \quad (37)$$

Since the first two parts on the right-hand side of Eq. 36 have constant values, the static pressure variation inside the bubble depends only on the velocity distribution and can be calculated using Eq. 37. Hence, we represent constant pressure lines by curves of constant velocity.

As the normal velocity varies at the bubble boundary, the pressure distribution has a step change. The pressure drop at the bubble boundary ($\lambda=\lambda_0$) when it is crossed from inside to outside can be written using Eqs. 22, 23, 30, and 31, as

$$\Delta P=\rho_g\,\frac{U_0^2}{2}\,\frac{\mu^2(\lambda_0^2-1)}{\lambda_0^2-\mu^2}\,[G(\lambda_0)-1]^2(1-\epsilon^2). \quad (38)$$

This expression can be useful for a future analysis of the solid particles' behavior at the bubble boundary.

Results and Discussion

The variation of the relative mean vertical velocity U_c/U_{mf} with h/b inside the bubble, as calculated by Eq. 20 is plotted in Figure 3. It is seen that for $h/b=1$ (the case of the spherical bubble) $U_c/U_{mf}=3$. This agrees with the result presented by Davidson and Harrison (1963). As h/b increases, we see a significant rise of U_c/U_{mf}. For example, it attains a value of 10 when h/b equals 3.2. Hence, at the channeling regimes of fluidization, when the shape of an elongated bubble may be approximated by that of the prolate ellipsoids of revolution, we observe the significant growth of the mean vertical velocity inside the bubble in comparison with the case of a spherical bubble.

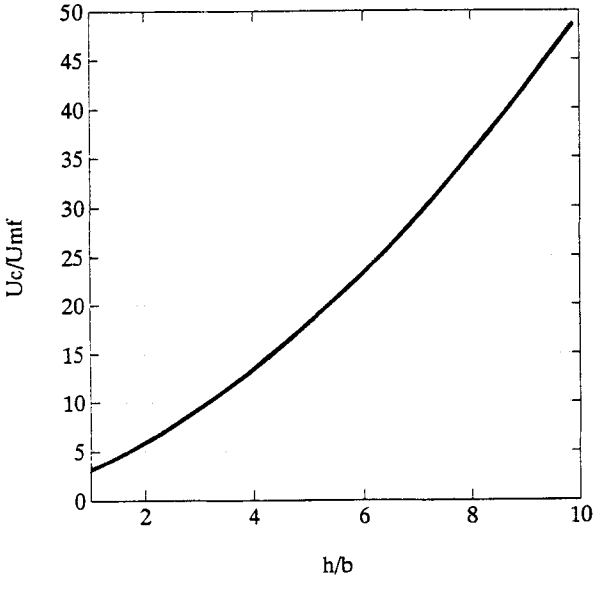

Figure 3. Relative mean vertical velocity, as a function of relative bubble height.

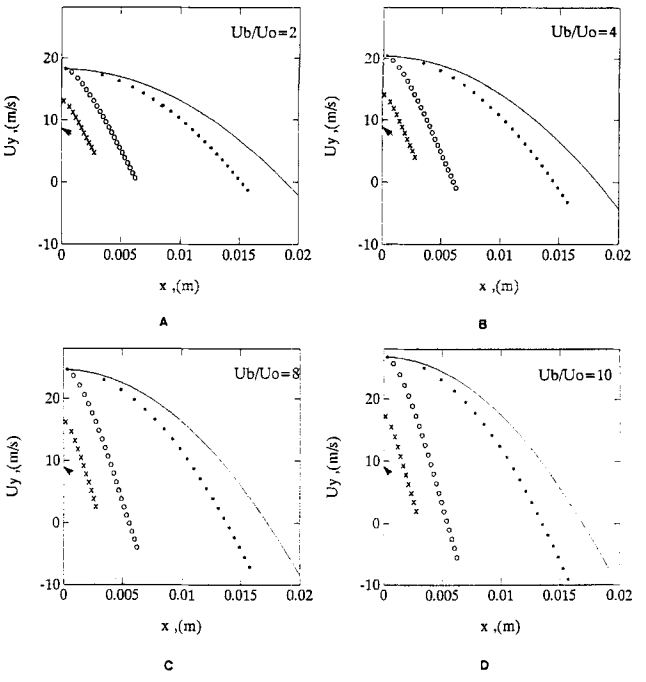

Figure 4. Vertical velocity distribution in elongated bubble cross sections.

With different values of relative Y-coordinate: —— $=0$; * * * $=0.6$; o o o $=0.95$; xxx $=0.99$; — 1; relative bubble height $h/b=5$.

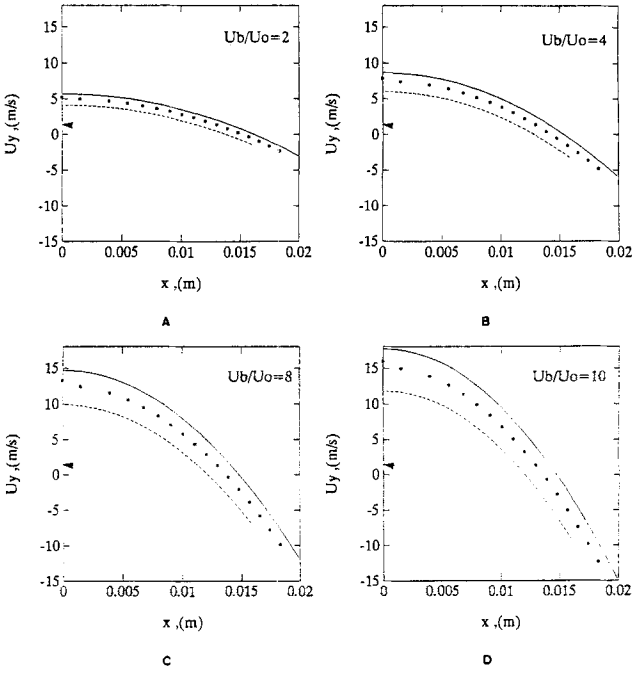

Figure 5. Vertical velocity distribution in spherical bubble cross sections.

With different values of relative Y-coordinate: —— $=0$; xxx $=0.4$; --- $=0.6$; — 1.

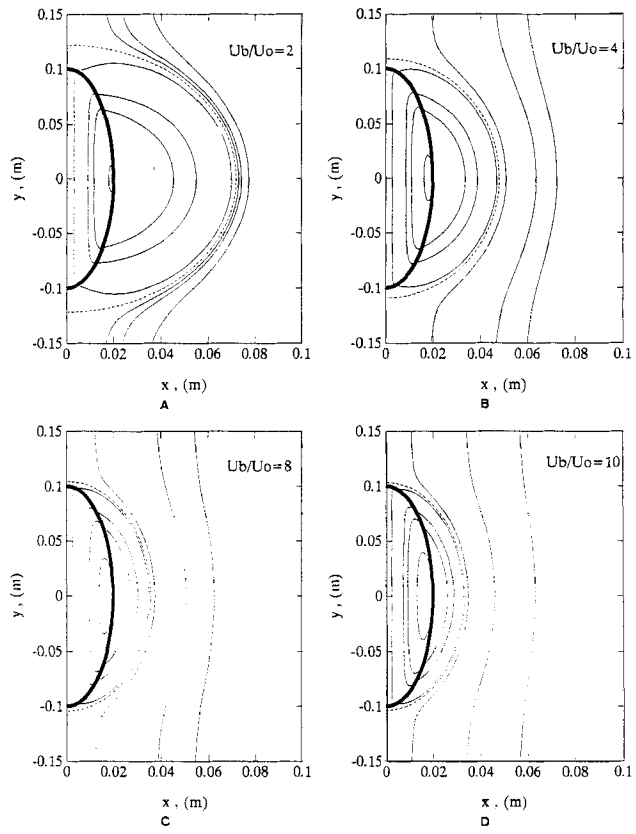

Figure 6. Stream lines inside and outside the elongated bubble.

Relative height $h/b=5$; --- surface of penetration.

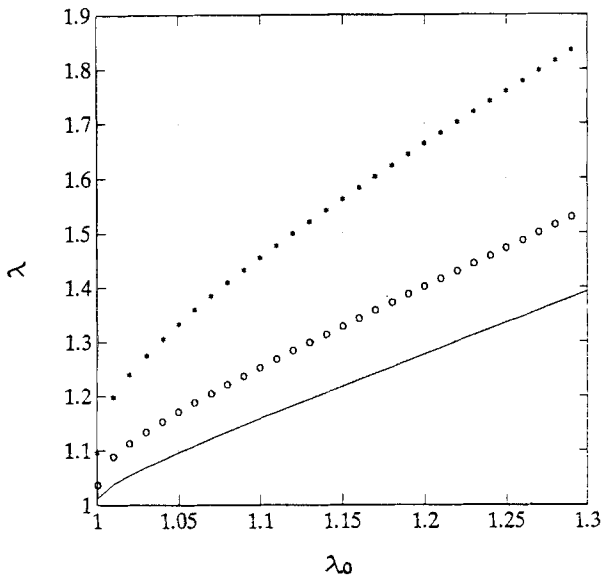

Figure 7. Connection between elliptic parameter λ of the surface of penetration and that of the bubble-λ_0.

Relative bubble velocities U_b/U_0: * * * = 2; o o o = 4; —— = 10.

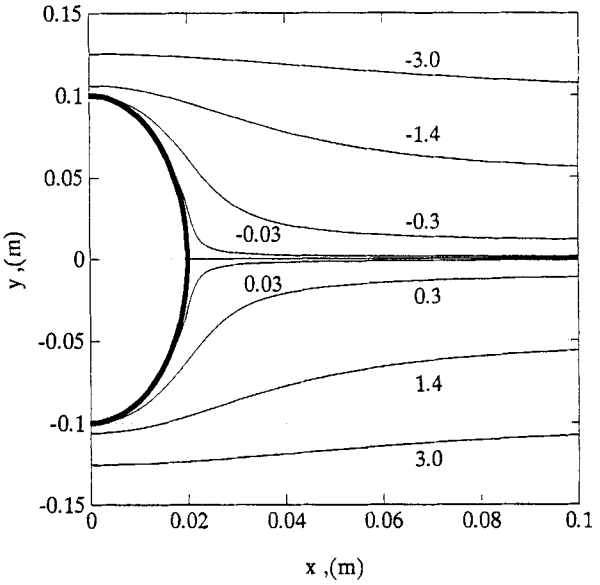

Figure 8. Constant relative stagnation pressure in (kPa) outside elongated bubble.

Relative height $h/b=5$, $U_b/U_0=2$.

The vertical velocity distributions across the bubble at different levels and for four values of U_b/U_0 are plotted in Figure 4a-d for elongated bubbles of $h/b=5$ and in Fig. 5a-d for spherical bubbles. Value $U_b/U_0=2$ corresponds to Figures 4a and 5a, $U_b/U_0=4$ to Figures 4b and 5b, $U_b/U_0=8$ to Figures 4c and 5c, and $U_b/U_0=10$ to Figures 4d and 5d. From the figures it can be seen that the maximum vertical velocity exists in the origin for spherical bubbles and along y-axes between the two foci ($c/h=0.979$) for the elongated bubble. Outside these points the velocity value decreases. The constant velocity value between foci is probably a result of the ellipsoid geometry properties and may not exist if one approximates the shape of the elongated bubble to another geometrical configuration. However, the velocity decrease toward the top point seems to be a common property of the bubbles.

We can see from these figures that the vertical velocity values in the elongated bubble exceed those in the spherical bubble. At the top points they are six times greater, in agreement with Figure 3. These maximum values can be calculated according to Eq. 20. In the origin the relation between the maximum vertical velocity in elongated and spherical bubbles increases with a decrease in the relative bubble velocity value U_b/U_0; it approaches the value of 6 for $U_b/U_0 \to 0$.

The stream lines inside and outside the elongated bubble are presented in Figures 6a-d. Figure 6a corresponds to the value $U_b/U_0=2$, Figure 6b to $U_b/U_0=4$, Figure 6c to $U_b/U_0=8$, and Figure 6d to $U_b/U_0=10$. The figure shows that increasing U_b/U_0 decreases the size of the surface of penetration and increases the internal circulation zone. The variation in the size of the surface of penetration of the elongated bubble (λ vs. λ_0) for different U_b/U_0, as described by Eq. 24, is given in Figure 7. The parameters λ, λ_0, shown in the figure, relate to the elliptic coordinates in Figure 1 by the equation

$$\zeta = \text{arccosh } \lambda.$$

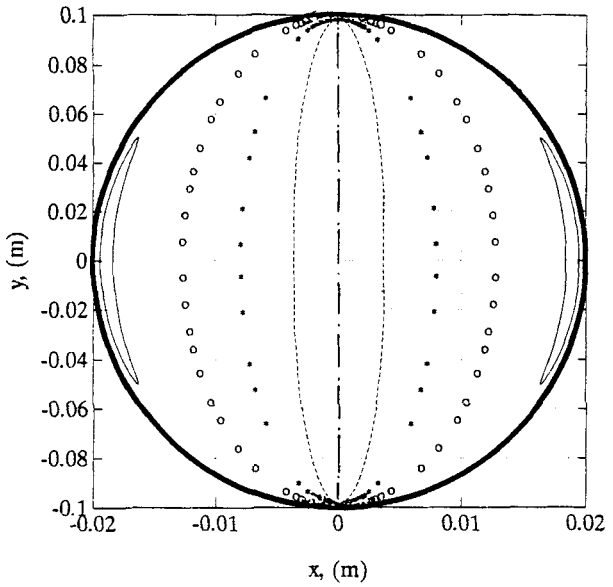

Figure 9. Constant relative static pressure (in kPa) inside elongated bubble.

$h/b=5$, $U_b/U_0=2$; relative static pressure: -·-·- = 0.2; ---- = 0.18; * * * = 0.13; o o o = 0.06; —— = 0.006.

The relative stagnation pressure distribution outside the bubble is calculated by Eq. 15 and is plotted in Figure 8. Figure 9 corresponds to constant relative static pressure lines inside the bubble (for the case of $U_b/U_0=2$). The results were obtained by calculating constant $|\overline{U}_i|$ values using Eq. 37 and are in accordance with the constant stagnation pressure inside the bubble (Eq. 36).

Acknowledgment

The research was supported by The Center for Absorption in Science, Ministry of Immigrant Absorption, State of Israel, as well as jointly by the Israeli Ministry of Science and Technology (MOST) and the German Bundesministerium fuer Forschung und Technologie (BMFT). We would also like to thank Dr. V. Sherbaum for some useful remarks concerning the aims of the research and the results presented in this paper.

Notation

A_n = constant coefficients in the solution of Laplace's equation
b = spherical bubble radius
c = eccentricity
$F(x)$ = $\frac{1}{2}\ln[(x+1)/(x-1)]-[x/(x^2-1)]$, mathematical function
$G(x)$ = $(1+1/[F(x)(x^3-x)])^{-1}$, mathematical function
g = 9.81 m/s^2
H = depth of the bubble center
h = semiheight of the bubble
κ = Darcy's law constant
P_o = stagnation pressure
$P_{b,s}$ = pressure above bed surface
P_f = pressure in the fluidized bed
$P_n(x)$ = Legendre functions of the first kind
$Q_n(x)$ = Legendre functions of the second kind
q = flow rate
r = circle's radius in the plane of the ellipse revolution
U = absolute gas velocity
U_b = bubble rising velocity
U_c = mean gas velocity inside the bubble
U_{mf} = superficial gas velocity at minimum fluidization
U_0 = interstitial gas velocity at minimum fluidization
$\overline{U}_b$ = U_b/U_0
$\overline{U}_{b_t}$ = $\overline{U}_b/\epsilon$
V = solid velocity
W = relative gas velocity
x, y = components of the right angle coordinate system
ϵ = voidage coefficient
ϕ = velocity potential
Ψ = stream function
ξ, η = components of the elliptic coordinate system
λ = cosh ξ
μ = cos η
ρ_g = gas density
ρ_p = solid particle density

Indices

i = inside the bubble
o = outside the bubble

Literature Cited

Davidson, J. F., "Symposium on Fluidization—Discussion," *Trans. Inst. Chem. Eng.*, **39**, 230 (1961).
Davidson, J. F., and D. Harrison, *Fluidized Particles*, Cambridge Univ. Press, London (1963).
Grace, J. R., and D. Harrison, "The Behavior of Freely Bubbling Fluidized Beds," *Chem. Eng. Sci.*, **24**, 497 (1969).
Happel, J., and H. Brenner, *Low Reynolds Number Hydrodynamics*, Prentice Hall, Englewood Cliffs, NJ (1965).
Lamb, H., *Hydrodyn.* (1945).
Pyle, D. L., and P. L. Rose, "Chemical Reaction in Bubbling Fluidized Beds," *Chem. Eng. Sci.*, **20**, 25 (1965).

Manuscript received December 2, 1993, and revision received Mar. 7, 1994.